Materials Science and Engineering C 42 (2014) 578–586

Contents lists available at ScienceDirect

Materials Science and Engineering C

journal homepage: www.elsevier.com/locate/msec

# Hydrothermal synthesis and thermal evolution of carbonate-fluorhydroxyapatite scaffold from cuttlefish bones

Emilija Tkalčec [a,*], Jasminka Popović [b], Sebastijan Orlić [a], Stjepan Milardović [a], Hrvoje Ivanković [a]

[a] Faculty of Chemical Engineering and Technology, University of Zagreb, Marulićev trg 19, Zagreb, Croatia
[b] Division of Materials Physics, Ruđer Bošković Institute, Bijenička 54, Zagreb, Croatia

ARTICLE INFO

*Article history:*
Received 19 December 2013
Received in revised form 4 May 2014
Accepted 29 May 2014
Available online 11 June 2014

*Keywords:*
Carbonated fluor/hydroxyapatite
Hydrothermal synthesis
FTIR
Thermal decomposition
XRD Rietveld structure refinement

ABSTRACT

Phase composition, crystal structure and morphology of carbonated fluor/hydroxyapatite synthesized hydrothermally from aragonitic cuttlefish bones were studied by powder X-ray diffraction (PXRD), Fourier transform infrared spectroscopy (FTIR), and scanning electron microscopy (SEM) combined with energy dispersive X-ray spectroscopy (EDS). The product of synthesis has been characterized as carbonated fluor/hydroxyapatite with carbonate incorporated inside channel (A-type) and substituted for the $PO_4^{3-}$ group (B-type). The vibration band at 874 $cm^{-1}$ assigned to bending ($\nu_2$) mode undoubtedly confirmed carbonate substituted for $PO_4^{3-}$ group, while the band at 880 $cm^{-1}$ was attributed to A-type carbonate substitution. The additional sharp and intense band at 865 $cm^{-1}$ considered as "non-apatitic" carbonate substitution is not assigned with certainty so far. Evolution of $CO_2$ from tetrahedral ($PO_4^{3-}$) sites with the increase in heat-treatment temperature is evident by the changes in tetrahedral bond lengths and angles, as obtained by the Rietveld structure refinement. Also, changes in the isotropic temperature parameters for the *2a* site point to A-type carbonate incorporation as well.



## 1. Introduction

Hydroxyapatite HA, $Ca_{10}(PO_4)_6(OH)_2$ has been shown to be chemically and crystallographically very similar, though not identical, to biologically formed hydroxyapatite [1–5]. The latter is nanosized carbonated hydroxyapatite (CHA), with incorporation of 3–6 wt.% of carbonate ions in its structure [6,7]. The carbonate ion can be incorporated inside channel (A-type) or can substitute for phosphate group (B-type). B-type CHA that most closely resembles the mineral phase of biological apatites has been extensively investigated; recent experimental and theoretical publications address the controversial subjects of the carbonate substitution, crystallographic structure and hydroxyl content of the bioapatites [8–17]. It is generally agreed that the planar carbonate ion substitutes for the phosphate tetrahedron in the B-type carbonated hydroxyapatite (CHA) and carbonated fluorapatite (CFA) structures, however, the question of the exact arrangement of the planar carbonate ion substituting for the tetrahedral phosphate has not been completely resolved yet [18]. This has become a major issue because detailed crystallographic structure properties are related to lattice modification caused by the carbonate substitution, the fractional atomic coordinates and the orientation of the carbonate group, i.e., parameters that consequently determine the physical properties of the materials. HA has a high dissolution rate in the biological system [19], poor corrosion resistance in an acid environment and poor chemical stability at high temperature [20], which has restricted its wider applications in the field of orthopedics and dentistry. It was suggested that fluorine-substituted hydroxyapatite (FHA), $Ca_{10}(PO_4)_6(OH)_{2-2x}F_{2x}$ where F replaces OH only partially, has better thermal and chemical stabilities than hydroxyapatite [21].

It is generally accepted that HA belongs to hexagonal crystal structure, space group $P6_3/m$ [1] with unit cell dimensions $a = 9.432$ Å and $c = 6.881$ Å, although very pure end member of HA crystallizes in monoclinic space $P2_1/b$ [6]. Fluorapatite, FA, belongs to the same space group as HA differing only in substitution of fluoride for the hydroxyl groups in HA structure. Since $F^-$ is smaller than $OH^-$, the substitution results in a contraction of the *a*-axis dimension to 9.368 Å, but with no significant change in the *c*-axis length ($a = 9.368$ Å, $c = 6.884$ Å; PDF# 15-0876). That phenomenon could be explained by considering the crystal structure of HA with randomly oriented $OH^-$ groups, which brings about a certain degree of disorder to the crystal structure. Once the $OH^-$ groups were partially substituted by the $F^-$ ions, the hydrogen of the $OH^-$ groups was bound to the nearby $F^-$ ions, producing a quite well ordered apatite structure, which caused an increase of the thermal and chemical stabilities of the HA matrix. However, it has been reported that if all of the $OH^-$ groups in HA are replaced by $F^-$ to form fluorapatite (FA), the resulting material is not osteoconductive [21]. Therefore, only a certain amount of $F^-$ ions should be substituted for the $OH^-$ groups forming fluorhydroxyapatite (FHA). Various methods have been developed in an attempt to tailor the fluorine content of FHA to achieve the best biological properties; such as precipitation [20], sol–gel [22], hydrolysis [23], mechanochemical [24] and

* Corresponding author. Tel.: +385 1 4597 219; fax: +385 14597 250.
*E-mail address:* etkalcec@fkit.hr (E. Tkalčec).

http://dx.doi.org/10.1016/j.msec.2014.05.079
0928-4931/

hydrothermal [25]. Hydrothermal conversion of biogenic aragonite to apatite has been successfully obtained using corals [26], cuttlefish bones [27–29], and nacres [30,31]. However, in that case carbonate hydroxyapatite (CHA), or carbonate fluorapatite (CFA) is formed. The formation of carbonated fluorhydroxyapatite should not be excluded too.

Cuttlefish bone (*Sepia officinalis*) was utilized as a source of biogenic calcium carbonate to prepare calcium phosphate scaffolds, mainly by several hydrothermal approaches. The aim of the scaffold-based bone tissue engineering is to repair and/or regenerate bone defects by using a scaffold as a platform for carrying cells or therapeutic agents to the site of interest. An ideal scaffold aims to mimic the mechanical and biochemical properties of the native tissue. In order to effectively achieve these properties a scaffold should have a suitable architecture favoring the flow of nutrients for cell growth. It should also have osteoconductive properties, supporting cells through a suitable surface chemistry [32,33]. To the best of our knowledge, Rocha et al. [27–29] were the first authors who transformed cuttlefish bones hydrothermally into hydroxyapatite tissue scaffolds retaining the cuttlebone architecture, noting that the channel sizes of the cuttlebone samples investigated were beneficial for bone in growth (~100 × 200 μm). A range of other benefits including good machinability were also recognized, indicating rather promising results. Kannan et al. [34] studied the transformation of aragonitic cuttlefish bones into fluorinated hydroxyapatite scaffolds with different levels of fluorine substitution (46% and 85%) on the $OH^-$ sites via hydrothermal transformation at 200 °C. Based on the Fourier transform infrared (FTIR) analysis, the authors declared nanosized AB-type, carbonated crystallites with unit cell parameters at 1200 °C typical for FA lattice, experiencing contraction along the *a*-axis rather than the *c*-axis.

One of the most outstanding features of nanocrystalline apatites of biological or synthetic origin is the presence of "non-apatitic" environments of the mineral ions [35]. These environments have been observed in some apatites [36,37], but not yet studied in species derived from cuttlefish bones. In this work we synthesized nanosized carbonated fluor/hydroxyapatite by hydrothermal treatment of cuttlefish bones, *S. officinalis*, from the Adriatic Sea. Compositional, structural and microstructural evolution of hydrothermally prepared fluor/hydroxyapatite during additional heat-treatment has been investigated. Changes of vibration bands for A- and B-substitution and "non-apatitic" carbonate with respect to applied heat treatment were monitored. Special attention was given to correlate the FTIR spectra and their characteristics with structural changes of crystalline phase induced by expelling carbonate, since the properties of the synthetic material are controlled by their crystallographic structure.

## 2. Materials and methods

### 2.1. Materials

The starting materials, pieces of native cuttlefish bones, *S. officinalis*, from the Adriatic Sea, were heated at 350 °C for 3 h, to remove the organic part of the shells. For hydrothermal treatment only pieces of cuttlefish bone from internal lamellae spacing were used, since by the pre-treatment at 350 °C the aragonite in external wall (dorsal shield) partially transforms into calcite, which further transforms into HA more difficult than aragonite [38]. Small pieces of bones (about 2 $cm^3$) were treated with the required volume of an aqueous solution of 0.6 M $NH_4H_2PO_4$ to set the Ca/P molar ratio to 1.67 and fluorine was introduced via $NH_4F$ solution to achieve stoichiometric level of substitution. Cuttlefish bone and the solutions were sealed in Teflon lined stainless steel pressure vessel and heated at 200 °C in step of 20 °C and dwelled for 24 h in an electric furnace. The pressure inside the reactor was self-generated by water vapor. The converted sample assigned as HT-25 was washed with boiling water and dried at 110 °C. Grinding of sample was accomplished with an agate mortar and pestle, to produce a fine powder that was used in thermal analysis, X-ray diffraction, and FTIR experiments.

### 2.2. Methods

Thermal behavior of the hydrothermally prepared sample was characterized by differential thermal analysis (DTA, Netzsch STA 409 analyzer). About 50 mg of the sample was placed in Pt crucible and heated at the rate of 10 K $min^{-1}$ in a synthetic air flow of 30 $cm^3$ $min^{-1}$ with α-alumina as a reference. In order to establish the structural evolution of phosphate phase with temperature, hydrothermally prepared and washed sample (HT-25) was heated in DTA apparatus up to 600 °C, 790 °C, 950 °C, 1100 °C and 1300 °C, respectively, and then cooled down with the cooling rate of the furnace. Sample codes: FA-600, FA-790, FA-950, FA-1100 and FA-1300 will be used for thermally treated specimens in further discussion to make a distinction between hydrothermally prepared origin and additionally heat-treated specimens.

The samples were studied by X-ray diffraction (XRD) analysis using a Shimadzu XRD 6000 diffractometer with CuKα radiation. Data were collected over a 2θ range between 10 and 110° 2θ in a step scan mode with steps of 0.02° and counting time of 4 s per step. For the purpose of unit cell parameter determination, as well as for quantitative phase analysis, silicon (99.999 wt.%, Aldrich) was added as an internal standard. Changes of crystal structure synthesized origin upon heating were followed by Rietveld structure refinement approach [39]. Topas 2.1 software [40] was used for the data evaluation. Data of Perdikatsis [41] were applied as a starting model for the refinement of fluorapatite. Polynomial model was used to describe the background. Diffraction profiles were described by Pseudo–Voigt function. During the refinement a zero shift, scale factor, half-width parameters (U, V, W), asymmetry parameters and peak shape parameters were simultaneously refined. Structural parameters, atomic coordinates and $B_{iso}$ for two Ca atoms (*4f* and *6h*), one P atom (*6h*), two mirror plane oxygen atoms O1 and O2 (*6h*), and one out of plane oxygen atom O3 (*12i*) were also refined. Infrared (IR) spectra of the samples were acquired using a Bruker Vertex 70 Fourier transform infrared (FTIR) spectrometer in ATR (attenuated total reflectance) mode. The samples were pressed on a diamond and the absorbance data were collected between 400 and 4000 $cm^{-1}$ with spectral resolution of 1 $cm^{-1}$ and 64 scans.

The sample morphology and microanalysis of phases have been examined by scanning electron microscopy (SEM, TESCAN VEGA TS5136LS) equipped with an energy dispersive X-ray spectrometer (Oxford INCA X-sight).

## 3. Results

### 3.1. Morphology and microstructure

The morphology of the hydrothermally prepared sample HT-25 is shown in Fig. 1. The hydrothermally transformed material (HT-25) perfectly preserved the morphology of the initial aragonitic cuttlefish bone, while its composition and structure completely changed. The lamellar matrix of cuttlefish bone consists of many horizontal thin sheets (lamellae) supported by transversal pillars that form chambers sealed from each other [38].

SEM image (Fig. 1a) shows that the chamber-like architecture of aragonitic cuttlefish bone is retained during the hydrothermal transformation into fluorapatite. Pillars are uniformly covered with nanosized particles of apatite (Fig. 1b). The higher resolution of image (Fig. 1c) indicates the existence of many uniform, "dandelion-like" microspheres assembled with radially oriented nanorods with an average diameter of about 200 nm and an average length of about 0.4 μm. SEM images of sintered scaffold at 1100 °C with overall structure (Fig. 1d), a pillar covered with sintered features (Fig. 1e) and its higher resolution image (Fig. 1f) exhibited porous and interconnected structure of the scaffold.

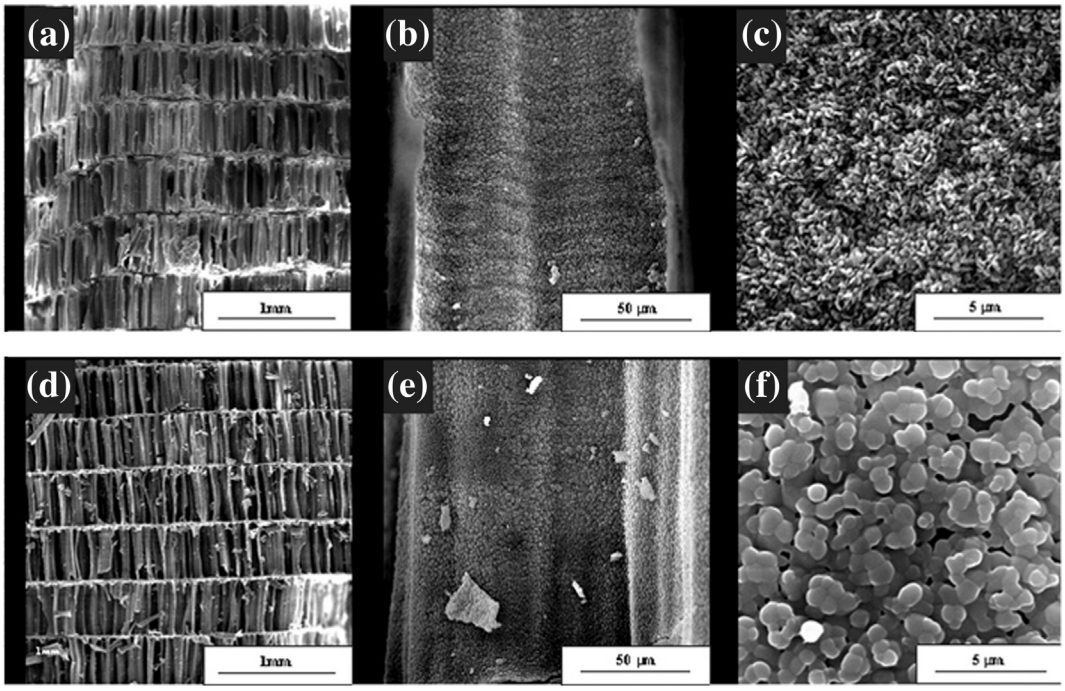


**Fig. 1.** SEM images of hydrothermally transformed aragonitic cuttlefish bones: (a) overall porous interconnecting structure; (b) pillars covered uniformly with "dandelion-like" microspheres of apatite; (c) higher magnification of "dandelion-like" microspheres; (d) SEM image of sintered scaffold at 1100 °C with overall structure; (e) a pillar covered with sintered acicular particles and (f) higher resolution of the previous image showing high porosity and interconnectivity of sintered particles about 2 μm in size.

### 3.2. Thermogravimetry

Thermogravimetric profile of the hydrothermally prepared sample and the associated first derivative curve are divided into five distinct steps (Fig. 2) and the mass loss in the each step is given in Table 1.

Adsorbed water is removed in the first step; not yet transformed aragonite completely decomposes up to 600 °C, while the mass loss in the range of 600–1100 °C (about 4.25 wt.%) could be attributed to the removal of carbon dioxide from the carbonated apatite (B-type and A-type substitutions) and "non-apatitic" carbonate, under the assumption that synthesis residuals [Eqs. (1) and (2)] were completely washed out from the sample.

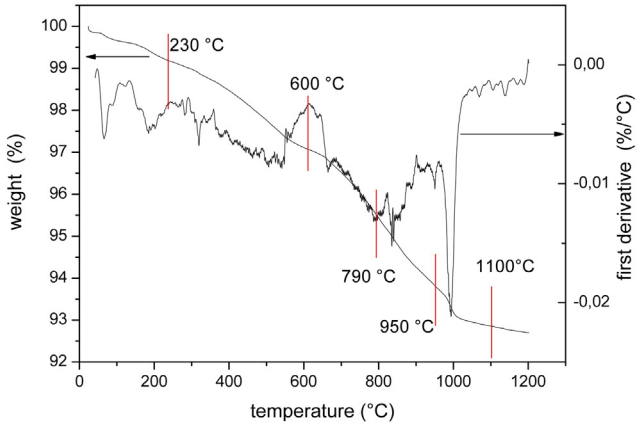


**Fig. 2.** Thermogravimetric (TG) curve of HT-25 sample and its associated first derivative thermogravimetric (DTG) curve. Perpendicular small bars were assigned for the temperatures where the analysis was stopped and the sample was cooled down to RT.

Chemical reactions of hydrothermal synthesis of fluor/hydroxyapatite and fluorapatite, respectively, can be described by Eqs. (1) and (2):

$$10CaCO_3 + 6NH_4H_2PO_4 + NH_4F + H_2O \rightarrow Ca_{10}(PO_4)_6(OH,F) + 3.5(NH_4)_2CO_3 + 6.5H_2CO_3 \quad (1)$$

$$10CaCO_3 + 6NH_4H_2PO_4 + 2NH_4F \rightarrow Ca_{10}(PO_4)_6F_2 + 4(NH_4)_2CO_3 + 6H_2CO_3. \quad (2)$$

### 3.3. FTIR spectroscopy

FTIR spectra of hydrothermally prepared HT-25 and heat-treated samples derived from HT-25 (Fig. 3) display the characteristic bands of nanocrystalline carbonated apatites [42]. Table 2 lists the present vibration modes of prepared samples, heat treated in temperature range 25–1300 °C; bands have been assigned according to literature data [17,21,35,38,42–51] and are cited in the table.

The band at 3570 $cm^{-1}$ in the high energy region regularly observed in HA structures due to the stretching mode of $OH^-$ ions is absent (Fig. 3a). The absence of $OH^-$ bonds on account of the carbonate content in the most carbonated CHA has also been confirmed by lack of band at about 631 $cm^{-1}$ [43]. The band at 3643 $cm^{-1}$ observed only at 1300 °C suggests the presence of $Ca(OH)_2$ [17,44]. After additional heat treatment at 550 °C the corresponding band (FA-1300 ht 550 in Fig. 3a) vanished. Considering the results of Rietveld quantitative analysis (see Section 3.4) the occurrence of vibration band of $Ca(OH)_2$ in FTIR is reasonable. CaO is frequently revealed in XRD patterns of heated nanocrystalline bioapatites [17,44], which further can readily hydrate to $Ca(OH)_2$. The band at 2325 $cm^{-1}$ is assigned to molecular $CO_2$ occluded on the surface of crystals [45].

The analysis of IR spectra in 400–1700 $cm^{-1}$ region (Fig. 3b) allows the identification of chemical environments of phosphate and carbonate ions. Phosphate groups related to stretching $\nu_3PO_4$ modes exhibited

**Table 1**
Decomposition steps of the hydrothermally prepared sample, DTG minima and mass losses in each step.

| Step | Temperature range (°C) | DTG minimum (°C) | Mass loss (wt.%) | Total sum of mass loss (wt.%) | Gases released from the sample |
|---|---|---|---|---|---|
| 1 | 25–230 | 198 | 0.79 | | Adsorbed water and synthesis residuals |
| 2 | 230–600 | 531 | 2.11 | 2.90 | Decomposition of aragonite and the rest of the synthesis residuals[a] |
| 3 | 600–790 | 790 | 1.54 | 4.44 | $CO_2$ release from carbonate apatite (B-type and A-type substitutions) and "non-apatitic" carbonate |
| 4 | 790–950 | 842 | 1.75 | 6.19 | $CO_2$ release from carbonate apatite (B-type and A-type substitutions) and "non-apatitic" carbonate |
| 5 | 950–1100 | 991 | 0.96 | 7.15 | $CO_2$ release from (B-type) carbonate apatite |

[a] Eqs. (1) and (2).

intense bands at 1026 $cm^{-1}$ and 1092 $cm^{-1}$ including the shoulders at 1067 and 1044 $cm^{-1}$ (seen only above 790 $cm^{-1}$ and 950 $cm^{-1}$, respectively). Bands at 600 $cm^{-1}$, 567 $cm^{-1}$, and 576 $cm^{-1}$ are related to $\nu_4PO_4$ bending modes. A weaker and narrower band at 965 $cm^{-1}$ is characteristic for the $\nu_1PO_4$ stretching mode, and the bending $\nu_2$ modes with frequency at 472 $cm^{-1}$ split into two bands above 790 °C.

Carbonate in apatite structure can be incorporated inside anionic channel (A-type) or substituted for $PO_4^{3-}$ (B-type) [48]. When carbonate ions replace tetrahedral $PO_4^{3-}$ sites, the infrared spectrum shows bands at about 1460, 1417 and 873 $cm^{-1}$ assignable to doubly degenerated stretching ($\nu_3$) and out of plane bending ($\nu_2$) modes of carbonate groups, respectively. On the other hand, in A-type substitution (where carbonate groups occupy OH or F positions) the $CO_3^{2-}$ stretching mode ($\nu_3$) normally appears at 1546 and 1456 $cm^{-1}$, and the bending mode ($\nu_2$) appears at 880 $cm^{-1}$. Consequently, the $\nu_3$ region comprises overlapped contributions from A and B carbonate species, therefore, the opinion that the ($\nu_2$) mode better reflects the true proportions of the principal carbonate species than ($\nu_3$) [51] was also considered within this article. Therefore, $\nu_2CO_3$ region has been deconvoluted by non-linear fitting (Fig. 4) and their spectral components analyzed for band position, width and area.

The band at 874 $cm^{-1}$ assigned to bending ($\nu_2$) mode undoubtedly confirms carbonate substituted for $PO_4^{3-}$ group (B-type substitution), while the band at 880 $cm^{-1}$ is attributed to A-type carbonate substitution. Furthermore, the band at 855 $cm^{-1}$ is ascribed to $\nu_2CO_3$ vibration mode of aragonite [52]. The presence of aragonite is confirmed from quantitative XRD analysis of HT-25 sample (see later). Recent advances in the characterization of apatite by FTIR spectroscopy have enabled to distinguish some additional bands in the characterization of nanocrystalline biological apatites and their synthetic biomimetic analogs that are not regular bands of apatites [53]. Therefore, the sharp and intense band at 865 $cm^{-1}$ could be considered as "non-apatitic" carbonate substitution, originating from the surface of nanoparticles [35]. However, it can be attributed to "francolite type" defect recently reported for natural fluorapatites that often established two different B-type substitutions: with frequency at 872 $cm^{-1}$ and at 865 $cm^{-1}$ [51,54]. Fleet [51] labeled the additional B-substitution as B2-type, although the specific assignment of the latter is not confirmed with certainty yet.

The characteristic vibration bands for A- and B-substitution in dependence of temperature are set apart from the other spectra in Fig. 5, while Fig. 6 depicts the changes of vibration bands for B-substitution and "non-apatitic"-substitution.

Fig. 7 shows the deconvoluted results of the position, width, and area of vibration bands with respect to heat treatment applied.

The $\nu_{2[B]}CO_3$ position (Fig. 7a) at 872 $cm^{-1}$ is shifted upwards and at 950 °C the shift yields about 3 $cm^{-1}$ (from 872 to 875 $cm^{-1}$). Further temperature increase does not influence the position of $\nu_{2[B]}CO_3$ band. No significant shift of peak positions of "non-apatitic" and A-type substitution was observed either. The peak width (Fig. 7b) diminished more intensively above 790 °C. $CO_3^{2-}$ is completely expelled from A-sites within 790 °C and 950 °C and from "non-apatitic" position within 950 and 1100 °C, while small amounts of $CO_3^{2-}$ ions in B-position can be determined even at 1100 °C. The temperature dependent ratio between the integrated intensities of different carbonate bands to the total carbonate, which actually expresses the fraction of corresponding modes, is given in Fig. 7d.

The degree of atomic ordering within the lattice with temperature, expressed by the width of the $\nu_1PO_4$ mode [47], has been correlated with the intensity ratio of $I(\nu_{2[B]}CO_3)/I(\nu_1PO_4)$ of the prepared fluorapatite and is shown in Fig. 8. It has been found that $\nu_1PO_4$ peak width changes with the same linearity as it is observed in natural carbonated fluorapatites [47].

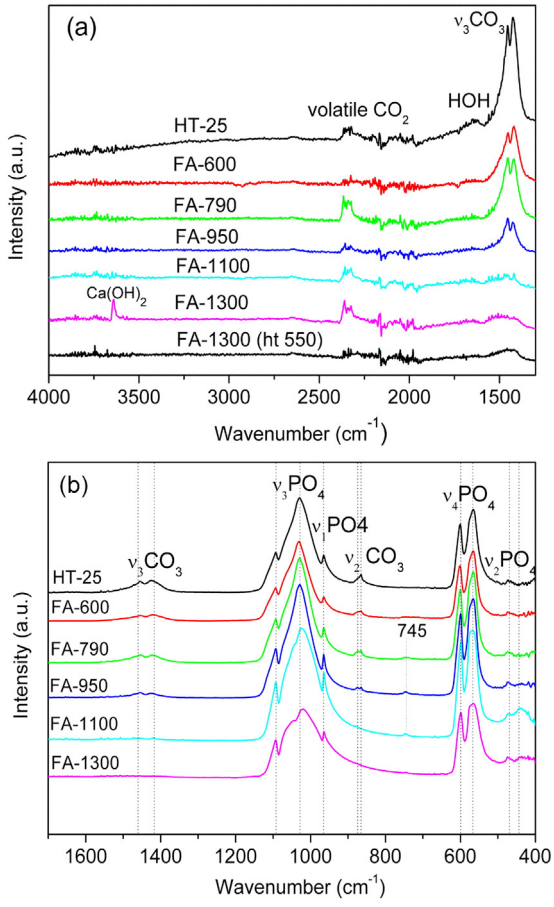


**Fig. 3.** (a) ATR FTIR spectra (hydroxyl region) of samples heat treated in temperature range from 25 to 1300 °C. The spectrum (ht 550) has been additionally heat treated at 550 °C before FTIR analysis; (b) ATR FTIR spectra (region of 400–1700 $cm^{-1}$) of samples heat treated in temperature range from 25 to 1300 °C.

### 3.4. XRD structural study

Sample HT-25 and specimens thermally treated at 600, 790, 950, 1100 and 1300 °C were characterized by means of X-ray powder diffraction (Fig. 9).

All samples contain, as a major crystalline phase, fluorhydroxyapatite (samples heat-treated in the range from 25 to 1100 °C) or fluorapatite (sample heat treated at 1300 °C). As a minor phase, sample

**Table 2**
Vibration modes for samples heat treated in temperature range 25–1300 °C and corresponding frequencies ($cm^{-1}$).

| Vibration mode | Assigned according to | HT-25 | FA-600 | FA-790 | FA-950 | FA-1100 | FA-1300 |
|---|---|---|---|---|---|---|---|
| $\upsilon_3PO_4^{3-}$ stretching | [42,43,47] | 1029, 1092 | 1029, 1092 | 1027, 1092, 1067[a] | 1026, 1092, 1067[a] 1044[a] | 1024, 1092, 1067[a], 1044[a] | 1019, 1092 1067[a], 1044[a] |
| $\upsilon_1PO_4^{3-}$ stretching | [47] | 964 | 965 | 965 | 965 | 965 | 964 |
| $\upsilon_4PO_4^{3-}$ bending | [47] | 599, 567, 576 | 600, 566, 576 | 600, 565, 576 | 600, 570, 573 | 600, 567, 570 | 600, 564, 570 |
| $\upsilon_2PO_4^{3-}$ bending | [47] | 472 | 472 | 467, 434 | 468, 440 | 468, 440 | 470, 434 |
| $\upsilon_3CO_3^{2-}$ stretching | [47–49] | 1460, 1417 | 1460, 1417 | 1458, 1424 | 1458, 1424 | 1460, 1450 | 1300–1600[b] |
| $\upsilon_2CO_3^{2-}$ bending | [48,50] | 872 (B-type) 880 (A-type) | 872 880 | 873 880 | 875 – | 875 – | – – |
| $\upsilon_2CO_3^{2-}$ "non-apatitic" bending | [35,51,54] | 864 | 864 | 865 | 865 | – | – |
| $CaCO_3$ (aragonite) | [38,52] | 856 | | | | | |
| OH···F | [21] | – | – | 745 | 745 | 745 | – |
| $Ca(OH)_2$ | [17,44] | – | | | | | 3643 |
| Gaseous $CO_2$[c] | [45] | 2322, 2357 | 2336 2365, | 2340 | 2325 | 2322, 2357 | 2336, 2365 |
| Water bending[d] | | 1630 | | | | | |

[a] Shoulder.
[b] Very broadened band overlapped in higher region.
[c] Additional band attributed to gaseous $CO_3^{2-}$.
[d] Band assigned to the presence of adsorbed water molecules on the crystallite surface.

HT-25 additionally contains a small amount of aragonite. With the increase in temperature aragonite decomposes, i.e. sample treated at 600 °C contains only apatite phase. With additional increase in temperature CaO starts to crystallize as a minor impurity phase (~1.2 wt.%) Appearance of CaO is frequently revealed in XRD patterns of heated nanocrystalline bioapatites [17,44].

Hexagonal $P6_3/m$ structure of fluorapatite ICSD no. 71-854 reported by Perdikatsis [41] was used as starting structural model for Rietveld refinements. Structure contains two Ca atoms (*4f* and *6h*), one P atom (*6h*), two mirror plane oxygen atoms O1 and O2 (*6h*), out of plane O3 atom (*12i*) and F atom in special position (*2a*). Although the presence of $OH^-$ anions, besides $F^-$ anions, is established by IR results, no hydroxyl anions are added to a structural model. Also a carbonate group was not included in the refinement as the difference between X-ray scattering factors for C and P is too small to distinguish between carbon and phosphorous atoms, especially when carbonate level is low. Nevertheless, the Rietveld refinement was useful for the determination of structural features of the phosphate group (bond distances and angles), which was indicated on the mode of carbonate incorporation in the original apatite structure. This hypothesis, about observed structural changes of phosphate group being caused by carbonate incorporation on phosphate group site, is justified by our findings from IR spectroscopy and is in accordance with the results of Leventouri [8–10] as well.

For the graphical result of Rietveld refinement for a chosen sample, sample FA-600 is given in Fig. 10.

The change in lattice parameters was noted with the increase in temperature; the unit-cell parameter *a* increased significantly and the *c*-lattice parameter decreased (Fig. 11).

Observed behavior of the unit-cell parameters is in accordance with literature data; pronounced increase of the unit-cell parameter *a* with the increase in temperature was also previously noted by other authors [10,41]. Rietveld refinement revealed significant changes in tetrahedral

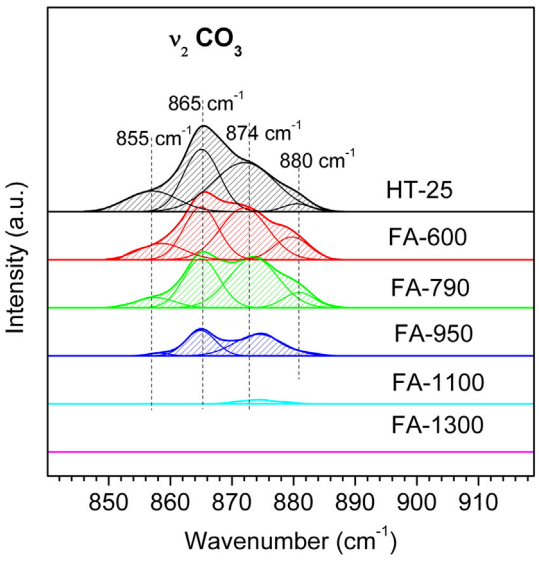


**Fig. 4.** FTIR spectra ($\nu_2CO_3$ regions) of samples heat treated in temperature range 25–1300 °C. The spectra are normalized. Vertical bars were assigned for the positions of vibration frequencies. The spectra are normalized in a way that the $\nu_1PO_4$ intensity remains constant and equals to unity.

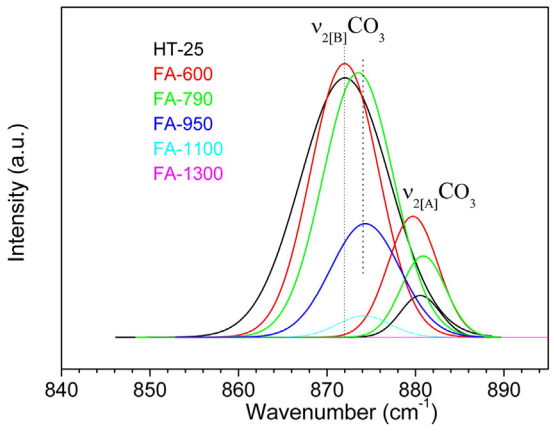


**Fig. 5.** Vibration bands $\nu_{2[A]}CO_3$ and $\nu_{2[B]}CO_3$ of samples heat treated in temperature range 25–1300 °C.

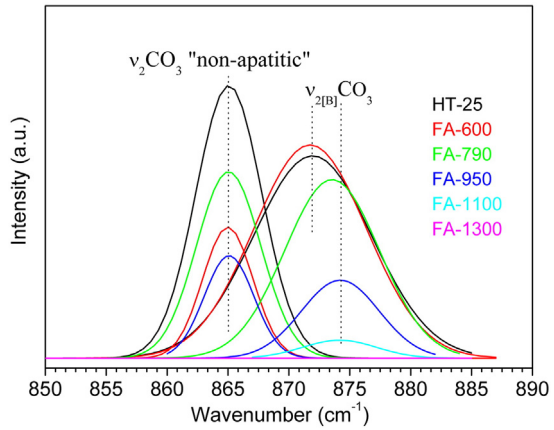


**Fig. 6.** Vibration bands $\nu_{2[B]}CO_3$ and "non-apatitic" $\nu_2CO_3$ of samples heat treated in temperature range 25–1300 °C.

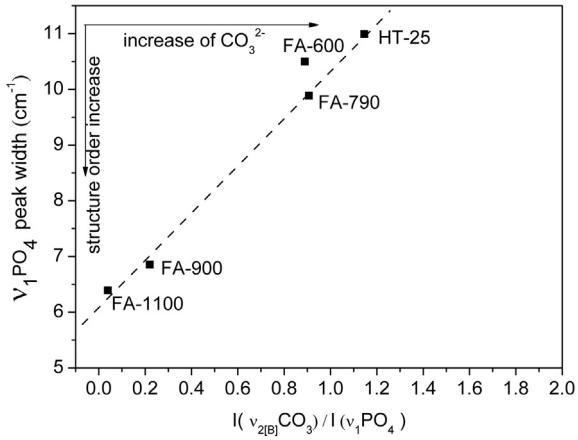


**Fig. 8.** The degree of atomic ordering within the lattice, as expressed by the width of the $\nu_1PO_4$ mode, versus the degree of carbonation (expressed by intensity ratio of $I(\nu_{2[B]}CO_3)/I(\nu_1PO_4)$ of the prepared fluorapatite.

bond lengths P–O1, P–O2 and P–O3 with the increase in the temperature of heat treatment (Fig. 12). Although *6h* site was refined without situating the carbon atom on it, the general notation T–O bonds, rather than P–O, will be used.

Fig. 12 depicts an increase of bond lengths T–O1 and T–O2, lying on the mirror plane, with the increase in temperature of heat treatment, while bonds T–O3, lying above and below mirror plane, decreased, as well as in-plane O1–T–O2 angle. Isotropic temperature parameters, $B_{iso}$, of atoms O1, O2, O3 and P are given in Fig. 13.

Carbonate rich sample, heat treated at low temperature, revealed a disturbance primarily at atom sites of phosphate group. Thermal factors, $B_{iso}$, of mirror plane atoms in carbonate rich sample (HT-25) are 3 times larger for O2, ~3.5 times larger for O1, and more than 7 times larger in the case of P atom, in comparison with the corresponding thermal factors in carbonate free samples (FA-1100, FA-1300). A noticeable disturbance (larger by factor ~1.5) is also observed for atom O3, due to created vacancy caused by $CO_3^{2-}$ substituting for $PO_4^{3-}$. Phase composition of the samples and chemical composition of the corresponding carbonate fluorapatites present in the samples, obtained by the Rietveld method are listed in Table 3. Besides quantitative phase analysis, Table 3 also lists the formula describing different apatite structures as a function of temperature as deducted by both XRD and IR results.

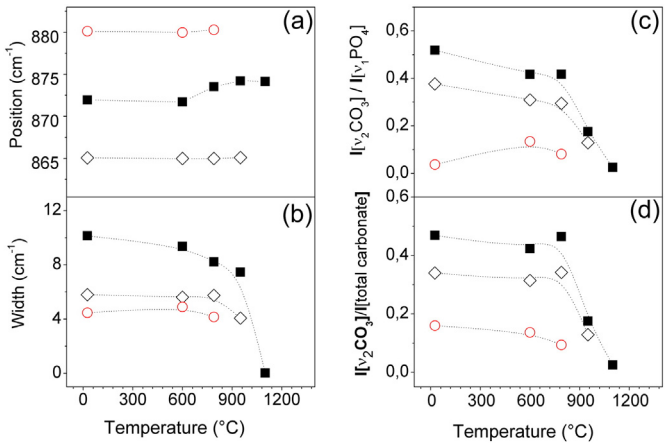


**Fig. 7.** (a) Peak positions of $\nu_{2[A]}CO_3$, $\nu_{2[B]}CO_3$ and "non-apatitic" $\nu_2CO_3$; (b) widths of corresponding modes; (c) the intensity ratios of the $\nu_2CO_3$ modes to the intensity of the $\nu_1PO_4$ mode; (d) the intensity ratio of different carbonate bands to the total carbonate. Squares are used for the $\nu_{2[B]}CO_3$, the open circles for the $\nu_{2[A]}CO_3$ modes and the open rhombs denote "non-apatitic" $\nu_2CO_3$ mode. For the purpose of clarity the intensity ratio of aragonite is not shown.

A-type substitution, as suggested based on FTIR data, was also considered during the structure refinement, however the refined occupancy for fluorine atom was associated with large e.s.d. (estimated standard deviation) and therefore excluded from further refinement.

Incorporation of carbonate in original apatite structure is also reflected by considerable lattice strain $e = 0.18\%$ observed for sample heat treated at lower temperatures. As carbonate content decreased, specifically for samples heat treated at 1100 and 1300 °C, which are considered to be carbonate-free, lattice strain becomes almost negligible. Size-strain analysis also revealed an increase of crystallite sizes as the carbonate content decreased. Fig. 14 shows the results of line-broadening analysis performed in the course of the Rietveld structure refinement.

## 4. Discussion

Aragonitic cuttlefish bones were hydrothermally converted into porous nanosized carbonated fluor/hydroxyapatite. The original microstructure of the cuttlefish bone was preserved by hydrothermal treatment as shown by SEM micrographs (Fig. 1), which featured >90% interconnected porosity. The synthesized origin HT-25 contains approximately 1 wt.% of aragonite not yet transformed, as determined by Rietveld structure refinement (Table 3); and no other crystalline phases were observed. Weight loss of 0.79% seen on TG curve (Fig. 2) suggests the presence of small amount of water, while there is no evidence for $OH^-$ groups in the structure on the results of infrared

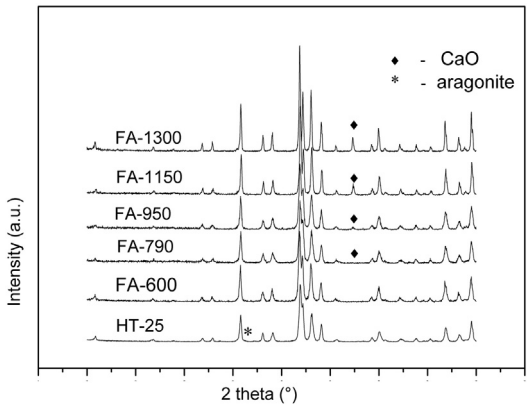


**Fig. 9.** PXRD patterns for sample HT-25 and samples thermally treated at 600, 790, 950, 1100 and 1300 °C.

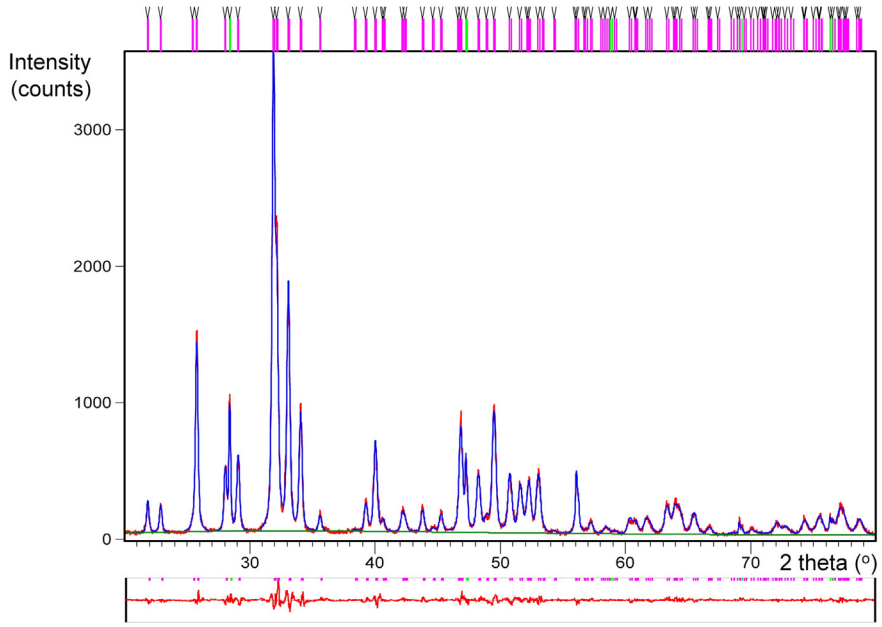


**Fig. 10.** Graphical result of the Rietveld refinement for sample heat treated at 600 °C; FA-600. The magenta vertical marks represent the positions of carbonated fluorapatite while green bars mark the diffraction lines of Si standard (used for zero shift correction). Experimental data are shown in red, the calculated pattern in blue while difference curve is given below the pattern. (For interpretation of the references to color in this figure legend, the reader is referred to the web version of this article.)

spectroscopy (Fig. 3, Table 2). In temperature treatment range from 230 to 1100 °C, the sample lost 6.36 wt.% (Table 2) from which ~4.25 wt.% is due to $CO_2$ incorporated into apatite structure, under the assumption that synthesis residuals [Eqs. (1) and (2)] were completely washed out from the sample.

The analysis of IR spectra in 400–1700 $cm^{-1}$ region (Fig. 3b) allows the identification of chemical environments of phosphate and carbonate ions. Especially the $\nu_2CO_3$ region of IR spectra most conveniently reveals specific carbonate substitution sites. Based on IR spectra (Figs. 4–7) the crystalline phase in the origin HT-25 should be considered as nanosized A and B carbonated fluorapatites (~50 nm in size) with carbonate incorporated within channels as well as at $PO_4^{3-}$ group sites. Although carbonate incorporation at both sites is undisputable from IR spectra an additional issue, regarding the presence of $OH^-$ and/or $F^-$ anions within the channel voids, can be raised since neither $OH^-$ nor OH···F bands (Fig. 3a and band at 745 $cm^{-1}$ in Fig. 3b) have been noticed. The evidence for the lack of $OH^-$ in the FA-600 is also undisputable. On the contrary, in specimens derived from the same origin and thermally treated at 790 °C, 950 °C and 1100 °C OH–F bonds were confirmed with certainty, suggesting both anions in channel sites. The absence of bands assigned to $OH^-$ vibrations in nanosized bioapatites and in their synthetic biomimetic analogs has been often reported [21,54]. The charge imbalance created by the replacement of one $PO_4^{3-}$ tetrahedral group by one $CO_3^{2-}$ group could be counter-balanced by creating a vacancy in the channel site [55]. Furthermore, hydroxyl ion concentration correlates inversely with carbonate content [17]. Accordingly, it is plausible to account for the lack of $OH^-$ only in HT-25 and FA-600 samples with far more carbonate present than in specimens heated at higher temperatures. By expelling carbonate from the channels at about 790 °C OH–F vibrations are well visible and detectable up to 1100 °C. Therefore, the apatite in the whole temperature range 25–1100 °C (Table 3) was declared as carbonated fluorhydroxyapatites, i.e., solid solutions consisting of end members of the apatite family (hydroxyapatite and fluorapatite).

At temperature 1300 °C carbonate from tetrahedral sites is entirely expelled fast and the renewed charge imbalance should be counter-

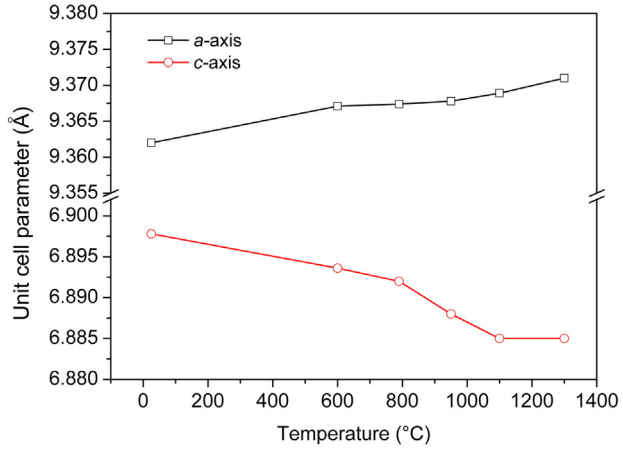


**Fig. 11.** Lattice parameters for samples heat treated in temperature range 25–1300 °C.

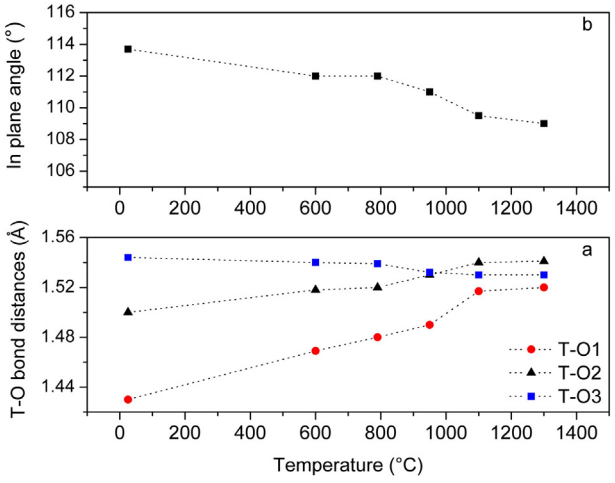


**Fig. 12.** Temperature dependence of tetrahedral bond lengths: (a) T–O1, T–O2 and T–O3; (b) in plane angle O1–T–O2.

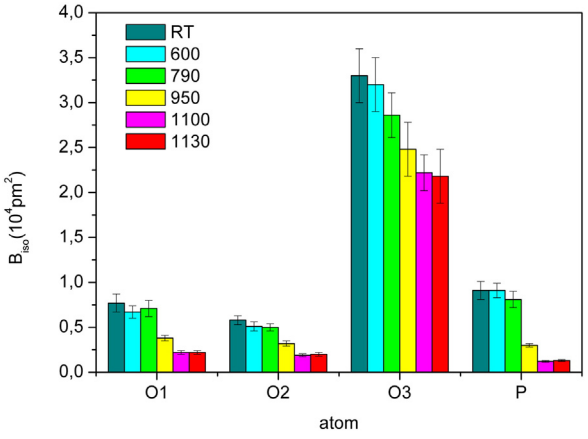


**Fig. 13.** Isotropic temperature parameters of selected atoms in crystal structure of samples heat treated in temperature range from 25 to 1300 °C.

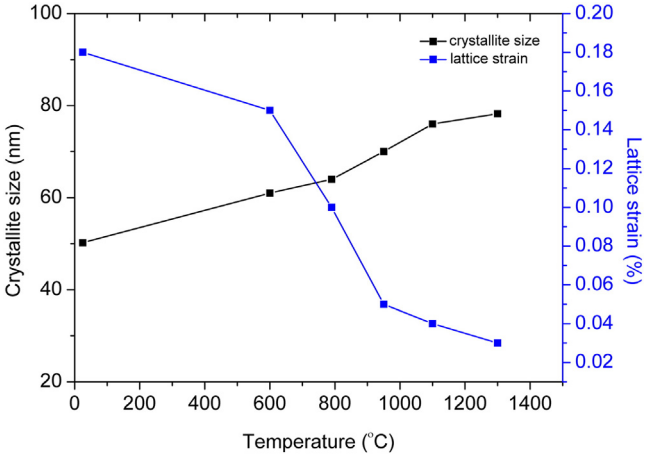


**Fig. 14.** Crystallite size and lattice strain of thermally treated samples.

balanced by rearrangement of the chemical species in channels; an OH–F bond becomes unstable. That temperature, in fact, marks an onset of fluorhydroxyapatite structure degradation, and since hydroxyl anions are weakly bonded (compared to $F^-$) they are first to leave the channel. Thermal decomposition of hydroxyapatites, where $OH^-$ anions are leaving the structure in the form of $H_2O$, is reported by Adolfsson and Hermansson [56]. Unexpected band at 3643 $cm^{-1}$ observed only at 1300 °C was attributed to the presence of $Ca(OH)_2$ [17,44]. Even a small amount of $Ca(OH)_2$ are known to be visible from IR spectra and still unrecognizable by means of X-ray diffraction. Accordingly, the assignation of the respective band to $Ca(OH)_2$ was reasonable. Its degradation occurs at 400 °C therefore the band disappears in IR spectrum of FA-1300 ht 550. Whether the dehydroxylation of fluorhydroxyapatite influences the formation of $Ca(OH)_2$ requires further study. The mutual interdependence of fluorhydroxyapatite dehydroxylation and the formation of $Ca(OH)_2$ could be presumed.

It is worth noting that thermally treated samples were derived from the same hydrothermally prepared origin with stoichiometrical ratio of calcium and phosphorus sources equal to 1.67 (in the range of experimental errors), therefore the possible mismatch providing hydrothermal synthesis is excluded. Accordingly, the amount of both Ca and P is constant and should be equal to the stoichiometric ratio in the whole range of thermal treatment. However, Ca/P ratio for crystalline apatite structure in sample HT-25 equals to 2.25 and with temperature increase $CO_2$ and other volatile components expelled from the structure, the phosphate content inside apatite increases, and Ca/P ratio approaches an ideal stoichiometric value for apatite of 1.67 (Table 3). In order to explain the different values in Ca/P ratio with an increase in temperature a structural model for nano-crystalline biological apatites, recently accepted by a significant number of researchers (see reviews [35,57] and references within) has to be considered. According to that model nano-crystalline biological apatites are covered by "non-apatitic" structured, but not crystalline hydrated domains containing relatively mobile ions (mainly bivalent cations and anions: $Ca^{2+}$, $CO_3^{2-}$, $HPO_4^{2-}$) and various volatile residuals, which can entrap phosphate ions not yet incorporated in the crystalline part of the apatite unit. Phosphate ions could also be captured within highly interconnected pores in the microstructure of cuttlefish bones preserved even by hydrothermal process (Fig. 1). Accordingly, a large amount of $PO_4^{3-}$ units are located outside of the crystalline structure.

It has to be emphasized that stoichiometric amount of fluorine was used for apatite synthesis. Thus, due to the participation of fluorine along with $OH^-$ groups in charge-compensation of carbonate in B-sites, it could be supposed that excess fluorine in non-channel positions could be utilized as candidate for charge compensation of "non apatitic" carbonate anions. Conclusively, the result obtained in this work, can also be in accordance with recently proposed composite carbonate–fluoride tetrahedron defect model given by Yi et al. [58] for experimentally observed IR absorption band at 864 $cm^{-1}$ in some natural fluorapatites.

Additional details on structural modes of carbonate incorporation were obtained from XRD results. Observed changes in tetrahedral bond lengths (Fig. 11) can be explained by partial replacement of phosphate group by planar carbonate group on the mirror plane of the apatite structure in samples heat-treated at lower temperatures. The same mode of carbonate incorporation was previously established in reports by Leventouri and co-authors [8–10]. Carbonate incorporation on mirror plane causes shortening of in plane tetrahedral bonds T–O1 and T–O2 due to atomic radius difference ($r$(C) = 1.2; $r$(P) = 1.8). Besides bond lengths, the in-plane angle was also affected by carbonate incorporation; since carbonate group is characterized by wider angle than phosphate group, substitution of phosphate by carbonate caused overall increment of O1–T–O1 angle in carbonate rich samples. Also, the substitution of tetrahedral $PO_4^{3-}$ by planar $CO_3^{2-}$ group created vacancies at O3 sites above and below mirror planes. Creation of oxygen vacancies caused enlargement of the channel size and therefore allowed more

**Table 3**
Composition of the prepared samples as determined by the Rietveld refinement. Formulas of the corresponding carbonate apatites as deducted by both XRD and IR.

| T (°C) | Sample composition (wt.%) | | | Carbonate apatite formula | Ca/P ratio in carbonate apatite |
|---|---|---|---|---|---|
| | Carbonate apatite | Aragonite | CaO | | |
| 25 | 99.0(1) | 1.0(2) | – | $Ca_{9.92}(PO_4)_{4.39}(CO_3)_{1.11}(OH,F,CO_3)_2$[a] | 2.25 |
| 600 | 100.0 | – | – | $Ca_{9.98}(PO_4)_{5.05}(CO_3)_{0.95}(OH,F,CO_3)_2$[a] | 1.98 |
| 790 | 98.8(1) | – | 1.2(1) | $Ca_{9.90}(PO_4)_{5.21}(CO_3)_{0.79}(OH,F,CO_3)_2$ | 1.90 |
| 950 | 98.9(1) | – | 1.1(1) | $Ca_{9.88}(PO_4)_{5.33}(CO_3)_{0.66}(OH,F,CO_3)_2$ | 1.85 |
| 1100 | 98.8(1) | – | 1.2(2) | $Ca_{9.94}(PO_4)_{5.80}(CO_3)_{0.2}(OH,F)_2$ | 1.71 |
| 1300 | 98.7(1) | – | 1.3(1) | $Ca_{9.9}(PO_4)_{5.91}(CO_3)_{0.09}F_2$ | 1.68 |

[a] The apatite phases are declared as A and B carbonated fluorhydroxyapatites although $OH^-$ and $F^-$ anions were not determined by IR analysis below 790 °C (see Discussion).

space for O3 atoms of unsubstituted phosphate groups, which is reflected as overall net expansion of T–O3 bonds in carbonate rich samples. As the carbonate is removed from the mirror plane of the structure by increasing the temperature of heat treatment, interatomic distances changed accordingly; removal of carbonate group with its shorter bond and wider angles contributed to overall increment of mirror plane bonds T–O1 and T–O2. Thus, the observed increment of lattice parameter *a*, as carbonate is driven off from apatite structure, is caused by expansion of the in-plane bonds while unit-cell parameter *c* decreased due to decrease of out-of-plane bond lengths. Besides geometrical parameters (bond lengths, bond angles) which confirmed carbonate substitution for phosphate group, the quantitative measure (Table 3) of the incorporation can be estimated from refined phosphorus atom occupancy of the *6h* site, $Occ(P_{6h})$, by assuming that carbon occupancy on that site, $Occ(C_{6h})$, equals $1\text{-}Occ(P_{6h})$.

Although XRD results are consistent with B-site substitution, a large isotropic temperature parameter of F site for carbonate rich samples ($B_{iso} = 3.8$ Å$^3$ in sample HT-25) when compared to those in carbonate-free samples ($B_{iso} = 1.1$ Å$^3$ in sample FA-1300) points at the presence of A-site substitution mode as well.

The observed lattice strain found in samples heat treated at lower temperatures (Fig. 14) resulted as a consequence of carbonate incorporation into original apatite structure (carbonate can be considered as defects) which prevented the crystallite growth. As carbonate is driven off, lattice strain becomes almost negligible promoting further crystal growth leading to noted increase in crystallite sizes.

## 5. Conclusion

Structurally ordered and stable up to 1300 °C fluorapatite can successfully be prepared by hydrothermally treated aragonitic cuttlefish bones with $NH_4H_2PO_4$ and $NH_4F$ as a source of phosphate and fluorine. Additional heat treatment can be used as simple method for targeted tailoring of carbonated fluor/hydroxyapatites with desired chemical composition as well as specific structural and microstructural features. Infrared spectroscopy can be used as an effective tool for tracking the decarbonation process in fluorapatites with respect to specific substitution site. Nevertheless, a Rietveld refinement of a simple structural model (without $CO_2$ groups) can also point to A- and B-substitution based on: i) specific changes in bond distances and angles within $PO_4$ groups (B-type) and ii) changes in thermal displacement parameters of *2a* site (A-type).

## Acknowledgment

The financial support of the Ministry of Science, Education and Sports of the Republic of Croatia in the framework of the project “Bioceramic, Polymer and Composite Nanostructured Materials” (no. 125-1252970-3005) is gratefully acknowledged. The technical assistance of Dr. V. Mandic is acknowledged.

## References

[1] L.Z. LeGeros, J.P. LeGeros, in: L.L. Hench, J. Wilson (Eds.), An Introduction to Bioceramics, World Scientific, Singapore, 1993, pp. 139–180, (Chapter 9).
[2] L.Z. LeGeros, Calcium Phosphates in Oral Biology and Medicine, Karger, Basel, Switzerland, 1991.
[3] M. Sadat-Shojai, M.T. Khorasani, E. Dinpanah-Khoshdargi, A. Jamshidi, Acta Biomater. 9 (2013) 7591–7621.
[4] M. Vallet-Regi, J.M. Gonzales-Calbet, Prog. Solid State Chem. 32 (2004) 1–31.
[5] M. Mazaheri, M. Haghighatzadeh, A.M. Zahedi, K.S. Sadrnezhaad, J. Alloys Compd. 471 (2009) 180–184.
[6] J.C. Elliot, Calcium phosphate biominerals, in: J.M. Kohn, J. Rakovan, J.M. Hughes (Eds.), Reviews in mineralogy and geochemistry, Phosphates: Geochemical, Geobiological and Material Importance, vol 48, Mineralogical Society of, America, Washington, DC, 2002, pp. 427–454.
[7] N. Roveri, M. Iafisco, Nanotechnol. Sci. Appl. 3 (2010) 107–125.
[8] T. Leventouri, B.C. Chakoumakos, N. Papanearchou, V. Perdikatsis, J. Mater. Res. 16 (2001) 2600–2606.
[9] T. Leventouri, B.C. Chakoumakos, N. Papanearchou, V. Perdikatsis, Mater. Sci. Forum 378 (2001) 517–522.
[10] T. Leventouri, B.C. Chakoumakos, H.Y. Moghaddam, V. Perdikatsis, J. Mater. Res. 15 (2000) 511–517.
[11] R.M. Wilson, J.C. Elliott, S.E.P. Dowker, R.I. Smith, Biomaterials 25 (2004) 2205–2213.
[12] M.E. Fleet, X. Liu, J. Solid State Chem. 177 (2004) 3174–3182.
[13] T.I. Ivanova, O.V. Frank-Kamenetskaya, A.B. Kol'tsov, V.L. Ugolkov, J. Solid State Chem. 160 (2001) 340–349.
[14] L. Rintoul, E. Wentrup-Byrne, S. Suzuki, L. Grøndahl, J. Mater. Sci. Mater. Med. 18 (2007) 1701–1709.
[15] D. Haverty, S.A.M. Tofail, K.T. Stanton, J.B. McMonagle, Phys. Rev. B 71 (2005) 094103–094109.
[16] G. Cho, Y. Wu, J.L. Ackerman, Science 300 (2003) 1123–1127.
[17] J.D. Pasteris, B. Wopenka, J.J. Freeman, K. Rogers, E. Valsami-Jones, J.A.M. van der Houwen, et al., Biomaterials 25 (2004) 229–238.
[18] T. Leventouri, Biomaterials 27 (2006) 3339–3342.
[19] M. Fini, L. Savarino, N. Nicoli Aldini, L. Martini, G. Giavaresi, G. Rizzi, D. Martini, et al., Biomaterials 24 (2003) 3183–3192.
[20] Y. Chen, X. Miao, Biomaterials 26 (2005) 1205–1210.
[21] L.M. Rodrıguez-Lorenzo, J.N. Hart, K.A. Gross, Biomaterials 24 (2003) 3777–3785.
[22] K. Cheng, S. Zhang, W. Weng, J. Sol–Gel Sci. Technol. 38 (2006) 13–17.
[23] E.Z. Kurmaev, S. Matsuya, S. Shin, M. Watanabe, R. Eguchi, Y. Ishivata, T. Takeuchi, et al., J. Mater. Sci. Mater. Med. 13 (2002) 33–36.
[24] H.G. Zhang, Q. Zhu, Z.H. Xie, Mater. Res. Bull. 40 (2005) 1326–1334.
[25] S. Jinawath, D. Polchai, M. Yoshimura, Mater. Sci. Eng. C 22 (2002) 35–39.
[26] B. Ben-Nissan, Curr. Opin. Solid State Mater. Sci. 7 (2003) 283–288.
[27] J.H.G. Rocha, A.F. Lemos, S. Kannan, S. Agathopoulos, J.M.F. Ferreira, J. Mater. Chem. 15 (2005) 5007–5011.
[28] J.H.G. Rocha, A.F. Lemos, S. Agathopoulos, P. Valerio, S. Kannan, F.N. Oktar, J.M.F. Ferreira, Bone 37 (2005) 850–857.
[29] J.H.G. Rocha, A.F. Lemos, S. Agathopoulos, S. Kannan, P. Valerio, J.M.F. Ferreira, J. Biomed. Mater. Res. 77 (2006) 60–168.
[30] C.M. Zaremba, D.E. Morse, S. Mann, P.K. Hansma, G.D. Stucky, Chem. Mater. 10 (1998) 3813–3824.
[31] A.F. Lemos, J.H.G. Rocha, S.S.F. Quaresma, S. Kannan, F.N. Oktar, S. Agathopoulos, J.M. F. Ferreira, J. Eur. Ceram. Soc. 26 (2006) 3639–3646.
[32] P.X. Ma, Mater. Today 7 (2004) 30–40.
[33] D.W. Hutmacher, Biomaterials 21 (2000) 2529–2543.
[34] S. Kannan, J.H.G. Rocha, S. Agathopoulos, J.M.F. Ferreira, Acta Biomater. 3 (2007) 243–249.
[35] J. Gómez-Morales, M. Iafisco, J.M. Delgado-López, S. Sarda, C. Drouet, Prog. Cryst. Growth Charact. Mater. 59 (2013) 1–46.
[36] C. Rey, B. Collins, T. Goehl, I.R. Dickson, M.J. Glimcher, Calcif. Tissue Int. 45 (1989) 157–164.
[37] C. Rey, V. Renugopalakrishnan, M. Shimizu, B. Collins, M.J. Glimcher, Calcif. Tissue Int. 49 (1991) 259–268.
[38] H. Ivankovic, H.G. Gallego Ferrer, E. Tkalcec, S. Orlic, M. Ivankovic, J. Mater. Sci. Mater. Med. 20 (2009) 1039–1046.
[39] R.A. Young, The Rietveld Method, International Union of Crystallography, Monographs on Crystallography, Oxford, 1993.
[40] The software TOPAS V 2, Advanced Bruker AXS, 2003. (Karlsruhe Germany).
[41] V. Perdikatsis, Mater. Sci. Forum 79–82 (1991) 809–814.
[42] J.C. Elliot, Structure and Chemistry of the Apatites and Other Calcium Orthophosphates, Elsevier, Amsterdam, 1994. (and references therein).
[43] G. Penel, G. Leroy, C. Rey, B. Sombret, J.P. Huvenne, E. Bres, J. Mater. Sci. Mater. Med. 8 (1997) 271–276.
[44] K.D. Rogers, P. Daniels, Biomaterials 23 (2002) 2577–2585.
[45] S.E.P. Dowker, J.C. Elliott, J. Solid State Chem. 47 (1983) 164–173.
[46] M. Wei, J.H. Evans, J. Mater. Sci. Mater. Med. 14 (2003) 311–320.
[47] A. Antonakos, E. Liarokapis, T. Leventouri, Biomaterials 28 (2007) 3043–3054.
[48] R.Z. LeGeros, O.R. Trautz, E. Klein, J.P. LeGeros, Experientia 25 (1969) 5–7.
[49] R.N. Panda, M.F. Hsieh, R.J. Chung, T.S. Chin, J. Phys. Chem. Solids 64 (2003) 193–199.
[50] G. Xu, I.A. Aksay, J.T. Groves, J. Am. Chem. Soc. 123 (2001) 2196–2203.
[51] M.E. Fleet, Biomaterials 30 (2009) 1473–1481.
[52] W.B. White, The carbonate minerals, in: V.C. Farmer (Ed.), The infrared spectra of minerals, Mineralogical Society of London Monograph, 1974, pp. 227–284.
[53] C. Rey, C. Combes, C. Drouet, H. Sfihi, A. Barroug, Mater. Sci. Eng. C 27 (2007) 198–205.
[54] M.G. Taylor, S.F. Parker, K. Simkiss, P.C.H. Mitchell, Phys. Chem. Chem. Phys. 3 (2001) 1514–1517.
[55] J.D. Pasteris, C.H. Yoder, M.P. Sternlieb, S. Liu, Mineral. Mag. 76 (2012) 2741–2759.
[56] E. Adolfsson, L. Hermansson, J. Mater. Sci. 35 (2000) 5719–5723.
[57] S.V. Dorozhkin, Am. J. Biomed. Eng. 2 (2012) 48–97.
[58] H. Yi, E. Balan, C. Gervais, L. Segalen, F. Fayon, D. Roche, A. Person, et al., Am. Mineral. 98 (2013) 1066–1069.